A Global Control Strategy for Efficient Control of a Braille Impact Hammer

Jenny Jerrelind
Division of Vehicle Dynamics,
Royal Institute of Technology,
SE-100 44 Stockholm, Sweden
e-mail: jennyj@kth.se

Harry Dankowicz
Engineering Science and Mechanics,
Virginia Polytechnic Institute
and State University,
Blacksburg, VA 24061

A combined control scheme relying on feedback-based local control in the vicinity of periodic system responses and global control based on a coarse-grained approximation to the nonlinear dynamics is developed to achieve a desirable dynamical behavior of a Braille printer impact hammer. The proposed control methodology introduces discrete changes in the position of a system discontinuity at opportune moments during the hammer motion while the hammer is away from the discontinuity, thereby exploiting the recurrent contacts with the discontinuity to achieve the desired changes in the transient dynamics. It is argued that, as the changes in the position of the discontinuity affect the motion only indirectly through changes in the timing and state at the subsequent contact, the control actuation can be applied over an interval of time during the free-flight motion as long as it is completed prior to contact. A forced, piecewise smooth, single-degree-of-freedom model of a Braille impact hammer is used to illustrate the methodology and to yield representative numerical results. [DOI: 10.1115/1.2159033]

1 Introduction

A Braille printer is an automated device that produces sequences of dots on paper representing Braille text for visually impaired persons [1,2]. Here, the motion of a movable mass is excited in order to generate repeated impacts between the mass and an anvil resulting in indentations in the paper being fed past the anvil. The quality of the resulting printout is reflected in the readability and durability of the dots. Low-velocity impacts result in weak dots that reduce readability. On the other hand, high-velocity impacts may result in holes in the paper. Moreover, if the movable mass is not retrieved from the anvil immediately following the impact, the motion of the paper past the anvil may result in tears. These observations impose constraints on the design and function of a Braille printer. Impact hammers similar to those used in a Braille printer are also common in matrix printers that apply color on paper to produce hard-copy computer output. Although the aim is not to generate measurable indentations in the paper, similar considerations apply to their design.

The presence of impacts results in an inherently nonlinear mechanical system, even when the excitation and the material response is linear. One would thus expect that Braille printers could exhibit highly irregular system responses, the coexistence of multiple system attractors, and bifurcations in system behavior (see [1,2], but also [3–5] in the case of matrix printers). The nonsmoothness originating in discontinuous changes in system state or forcing due to impacts could further result in discontinuity-driven bifurcations, such as those associated with grazing, zero-velocity contact.

Improvements in the function of impact-hammer-based printing devices may be achieved through passive redesign of system properties or the active imposition of feedback control (e.g., [2,6,7]). A typical design objective may be to increase the rate at which impacts can be generated (and thus the printing speed), while maintaining print quality.

The purpose of this paper is to outline a control strategy of a Braille impact hammer that presupposes the coexistence of multiple recurrent system responses and exploits the presence of discontinuities for affecting their stability. The paper proposes improvements in a previously studied local control algorithm [2,7] and appends this to a global control strategy based on a coarse discretization of the system dynamics.

The paper is organized as follows. Section 2 presents a brief review of the model formulation and its dynamics. The control methodology is developed in Sec. 3, followed by representative numerical results in Sec. 4 and a concluding discussion in Sec. 5.

2 Mathematical Model

Following Jerrelind and Dankowicz [2], the motion of the impact hammer is modeled using a single-degree-of-freedom system, see Fig. 1. Here, the spring-loaded core is excited by an electromagnetic force generated by a current pulse through a surrounding coil. Collisions with the front and back stops are modeled as perfectly inelastic impacts with associated changes in the total moving mass.

To account for the explicit time dependence of the system forcing, let the state of the dynamical system governing the impact hammer be given by

$$\mathbf{x} = (x\ \dot{x}\ t)^T, \tag{1}$$

where x denotes the hammer's horizontal displacement, $\dot{x}$ is its horizontal velocity, and t is time. The dynamics of the hammer are modeled through a combination of smooth changes in the state described by appropriate differential equations and discontinuous changes in the state associated with the transitions between free-flight motion and contact with the front or back stop, respectively. Specifically, we introduce two *event functions*

$$h_{\mathrm{fs}}(\mathbf{x}) = x - s, \tag{2}$$

$$h_{\mathrm{bs}}(\mathbf{x}) = x - \sigma, \tag{3}$$

whose zero-level surfaces in state space correspond to the onset and termination of contact with the front and back stop, respectively. Here, we assume that crossings of the zero-level surface of h_{fs} for $\dot{x} > 0$ result in discrete changes in the state given by the *jump function*

Contributed by the Technical Committee on Vibration and Sound of ASME for publication in the JOURNAL OF VIBRATION AND ACOUSTICS. Manuscript received March 10, 2004; final manuscript received May 11, 2005. Assoc. Editor: William W. Clark.

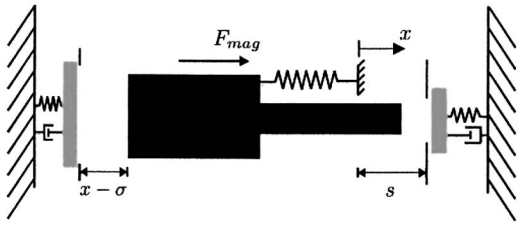

Fig. 1 Schematic model of the Braille printer impact hammer

$$\mathbf{g}_{\text{front impact}}(\mathbf{x}) = \begin{pmatrix} x & \frac{m_{\text{core}}}{m_{\text{core}}+m_{\text{fs}}}\dot{x}\ t \end{pmatrix}^T, \tag{4}$$

where m_{core} and m_{fs} are the masses of the core and front stop, respectively. Similarly, crossings of the zero-level surface of h_{bs} for $\dot{x}<0$ result in discrete changes in the state given by the jump function

$$\mathbf{g}_{\text{back impact}}(\mathbf{x}) = \begin{pmatrix} x & \frac{m_{\text{core}}}{m_{\text{core}}+m_{\text{bs}}}\dot{x}\ t \end{pmatrix}^T, \tag{5}$$

where m_{bs} is the mass of the back stop.

The differential equations governing smooth changes in the state are given by the vector field

$$\mathbf{f}(\mathbf{x}) = \begin{pmatrix} \dot{x} \\ \frac{1}{m_{\text{eff}}}(F_{\text{spring}} + F_{\text{mag}} + \{h_{\text{fs}} > 0\}F_{\text{fs}} + \{h_{\text{bs}} < 0\}F_{\text{bs}}) \\ 1 \end{pmatrix}, \tag{6}$$

where

$$m_{\text{eff}} = m_{\text{core}} + \{h_{\text{fs}} > 0\}m_{\text{fs}} + \{h_{\text{bs}} < 0\}m_{\text{bs}}, \tag{7}$$

$$F_{\text{spring}} = -k(x + d_{\text{spring}}), \tag{8}$$

$$F_{\text{mag}} = I^2(t)(L_1 x + L_0), \tag{9}$$

$$F_{\text{fs}} = -k_{\text{fs}}(x - s + d_{\text{fs}}) - c_{\text{fs}}\dot{x}, \tag{10}$$

$$F_{\text{bs}} = -k_{\text{bs},1}(x-\sigma)^2 - k_{\text{bs},2}(x-\sigma) - c_{\text{bs}}\dot{x}, \tag{11}$$

and the Boolean expressions evaluate to 1 when true and 0 otherwise. The terms d_{spring} and d_{fs} refer to the preload of the spring and the front stop, respectively. A graph of the form of the current pulse $I(t)$ is presented in Fig. 2. For numerical values of the parameters used in the discussion below see Table 1.

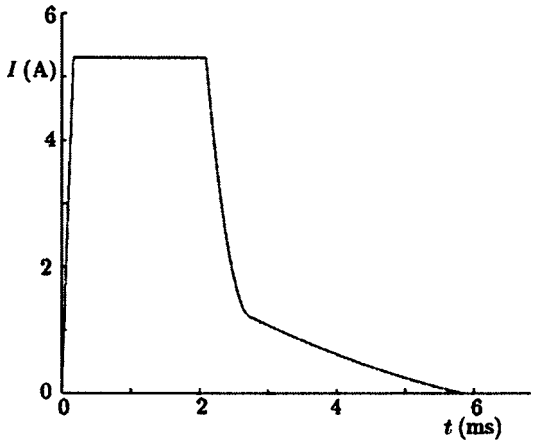

Fig. 2 Approximated current pulse [2]

Table 1 Specification of parameters for the Braille printer model [2]

Parameter	Value
m_{core}	4.46 g
m_{fs}	1.22 g
m_{bs}	2.16 g
k	100 N/m
k_{fs}	335e3 N/m
$k_{\text{bs},1}$	5e8 N/m^2
$k_{\text{bs},2}$	4e4 N/m
c_{fs}	37 N/s
c_{bs}	60 N/s
s	0.00328
σ	0 m
d_{spring}	0.002 m
d_{fs}	0.0002 m
L_0	0.16798 N/A^2
L_1	30.845 N/A^{2}m

The formulation above in terms of a smooth dynamics described by the vector field $\mathbf{f}$ and discrete dynamics described by the event functions h_{bs} and h_{fs} and the associated jump functions $\mathbf{g}_{\text{back impact}}$ and $\mathbf{g}_{\text{front impact}}$, respectively, can be easily implemented in MATLAB using the built-in event-handling routines.

The maximum rate at which dots may be generated is limited by the minimum lag time T_{lag} between subsequent pulses. Figure 3 shows the steady-state impact-hammer dynamics that result from a periodic excitation under variations in T_{lag} for $\sigma=0$. Here, large values of T_{lag} correspond to a periodic system response of the same period as that of the excitation. As T_{lag} is decreased, stability is lost at a cyclic fold bifurcation, after which the system exhibits a highly irregular response. As indicated in the figure, it is possible to delay the onset of the irregular motions by statically shifting the back stop in the direction of the paper, i.e., increasing σ.

3 Control Methods

The numerical results presented above reflect the response of the impact hammer to a periodic excitation. This is in contrast to the typical excitation used in practice, where a preselected sequence of current pulses is used to produce dots according to a

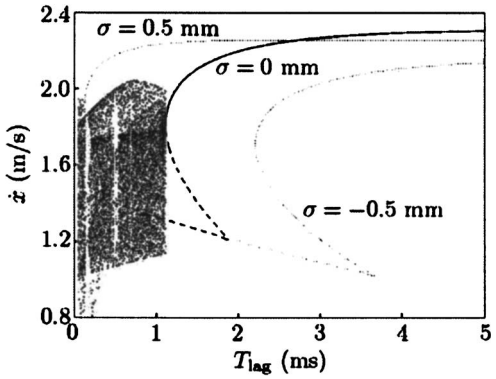

Fig. 3 Bifurcation diagram of the steady-state response of the impact hammer to a periodic current pulse under variations in lag time T_{lag}. Here, the gray curves indicate the shift of the periodic-trajectory bifurcation curves under variations in the position of the back stop, σ.

desired pattern. There, T_{lag} is chosen such that the hammer is allowed to come to rest against the back stop (as a result of a large dissipation of energy in the collision with the back stop) prior to the following pulse. This ensures a repeatable starting condition and guarantees that a high-quality dot may be generated per pulse. Contrary to the steady-state results in Fig. 3, the current operating paradigm thus relies primarily on transient dynamics.

An alternative to the design based on the transient system response is provided by considering the use of feedback control to switch between different steady-state motions under periodic excitation with different impact velocities. For example, Fig. 3 shows the coexistence of multiple periodic system responses (stable and unstable) corresponding to low- and high-velocity impacting motions over certain ranges in T_{lag}. The feedback algorithm could then be designed to guide the actual response between these periodic motions and thus switch between impacts that result in readable dots and impacts that do not.

Here it is proposed to control the observed dynamics of the impact hammer by exploiting the regular impacts between the hammer and the back stop. In particular, feedback-based, discrete changes in the position of the back stop that are introduced at opportune moments during the hammer's free-flight phase may have significant effect on the impact velocity following the next contact between the hammer and the back stop. Indeed, the suggested changes do not directly affect the system dynamics at the time that they are made. Instead, it is only by affecting the timing of the subsequent contact, the resultant change in momentum, and the timing of the release from the back stop that the imposed change indirectly controls the system dynamics.

From the above observations, it follows that the changes in the position of the back stop may be modeled as instantaneous, as long as they are completed before contact occurs. Finally, as the proposed control strategy relies on contact between the hammer and the back stop, it has no effect on trajectories that fail to impact the back stop.

3.1 Local Control. In a previous paper ([2], see also [7]), a control strategy was introduced to affect the local stability characteristics of a periodic system response of the impact hammer. There, discrete changes were made to σ—the value of x that corresponds to the onset and termination of contact between the hammer and the back stop—whenever the state reached a Poincaré section $\mathcal{P}_{\text{control}}$ given by the zero-level surface of the event function

$$h_{\text{control}}(\mathbf{x}) = x - d, \tag{12}$$

for some constant $\sigma < d < s$. Specifically, the control law

$$\sigma \to \sigma^{\text{ref}} + \mathbf{c} \cdot (\mathbf{x} - \mathbf{x}^*) \tag{13}$$

was considered, where σ^{ref} is a preselected reference value for the position of the back stop, $\mathbf{c}$ is a row matrix of gain parameters, and $\mathbf{x}^*$ is a comparison state on $\mathcal{P}_{\text{control}}$. Given a periodic trajectory that intersected $\mathcal{P}_{\text{control}}$ transversally in the point $\mathbf{x}^{\text{ref}}$, the goal was to find optimal values for the entries of $\mathbf{c}$ and a suitable method for selecting $\mathbf{x}^*$ that would achieve a desirable objective in terms of the local stability of the periodic motion.

Two local control strategies were proposed in [2], referred to as *reference feedback* and *delay feedback*. In the case of reference feedback, the comparison state $\mathbf{x}^*$ was chosen to equal the known quantity $\mathbf{x}^{\text{ref}}$. In contrast, in the case of delay feedback, the comparison state $\mathbf{x}^*$ was chosen to equal the value of $\mathbf{x}$ at the previous intersection with the Poincaré section $\mathcal{P}_{\text{control}}$. As this did not require knowledge of $\mathbf{x}^{\text{ref}}$, it was suggested that delay feedback would result in a more robust control strategy.

To analyze the effect of the control strategy on the local stability of the periodic trajectory, the augmented state

$$\tilde{\mathbf{x}} = (\mathbf{x}\ \sigma\ \mathbf{x}^*)^T. \tag{14}$$

is introduced. Smooth changes in $\tilde{\mathbf{x}}$ are then described by the augmented vector field

$$\tilde{\mathbf{f}}(\tilde{\mathbf{x}}) = (\mathbf{f}(\mathbf{x}, \sigma)\ 0\ \mathbf{0})^T \tag{15}$$

In addition to the discrete changes in $\tilde{\mathbf{x}}$ associated with the onset of contact with the front and back stop, respectively, an additional discrete change in $\tilde{\mathbf{x}}$ will now occur whenever the trajectory crosses $\mathcal{P}_{\text{control}}$ for $\dot{x} > 0$ given by the jump function

$$\tilde{\mathbf{g}}_{\text{control}}(\tilde{\mathbf{x}}) = (\mathbf{x}\ \sigma^{\text{ref}} + \mathbf{c} \cdot (\mathbf{x} - \mathbf{x}^*)\ \mathbf{x}^*)^T \tag{16}$$

in the case of reference feedback and

$$\tilde{\mathbf{g}}_{\text{control}}(\tilde{\mathbf{x}}) = (\mathbf{x}\ \sigma^{\text{ref}} + \mathbf{c} \cdot (\mathbf{x} - \mathbf{x}^*)\ \mathbf{x})^T \tag{17}$$

in the case of delay feedback.

Let $\tilde{\mathbf{x}}^{\text{ref}} = (\mathbf{x}^{\text{ref}}\ \sigma^{\text{ref}}\ \mathbf{x}^{\text{ref}})^T$. Then, in the absence of the discrete changes in $\tilde{\mathbf{x}}$ due to $\tilde{\mathbf{g}}_{\text{control}}$, the system dynamics near the given periodic trajectory can be described by the Poincaré map

$$\tilde{\mathbf{P}}(\tilde{\mathbf{x}}) = (\mathbf{P}(\mathbf{x}, \sigma)\ \sigma\ \mathbf{x}^*)^T, \tag{18}$$

for which

$$\tilde{\mathbf{P}}(\tilde{\mathbf{x}}^{\text{ref}}) = \tilde{\mathbf{x}}^{\text{ref}}. \tag{19}$$

In fact, even in the presence of the discrete changes in $\tilde{\mathbf{x}}$ due to $\tilde{\mathbf{g}}_{\text{control}}$,

$$\tilde{\mathbf{P}} \circ \tilde{\mathbf{g}}_{\text{control}}(\tilde{\mathbf{x}}^{\text{ref}}) = \tilde{\mathbf{P}}(\tilde{\mathbf{x}}^{\text{ref}}) = \tilde{\mathbf{x}}^{\text{ref}}, \tag{20}$$

i.e., the existence of the periodic trajectory is not affected by the proposed control.

In the absence of control, the local flow near the periodic trajectory is to lowest order captured by the matrix

$$\tilde{\mathbf{P}}_{\tilde{\mathbf{x}}}(\tilde{\mathbf{x}}^{\text{ref}}) = \begin{pmatrix} \mathbf{P}_{\mathbf{x}}^{\text{ref}} & \mathbf{P}_{\sigma}^{\text{ref}} & 0 \\ 0 & 1 & 0 \\ 0 & 0 & Id \end{pmatrix}, \tag{21}$$

where $\mathbf{P}_{\mathbf{x}}^{\text{ref}} = \mathbf{P}_{\mathbf{x}}(\mathbf{x}^{\text{ref}}, \sigma^{\text{ref}})$ and $\mathbf{P}_{\sigma}^{\text{ref}} = \mathbf{P}_{\sigma}(\mathbf{x}^{\text{ref}}, \sigma^{\text{ref}})$. In the presence of control, the corresponding matrices are

$$\tilde{\mathbf{P}}_{\tilde{\mathbf{x}}}(\tilde{\mathbf{x}}^{\text{ref}}) \cdot \tilde{\mathbf{g}}_{\text{control},\tilde{\mathbf{x}}}(\tilde{\mathbf{x}}^{\text{ref}}) = \begin{pmatrix} \mathbf{P}_{\mathbf{x}}^{\text{ref}} + \mathbf{P}_{\sigma}^{\text{ref}} \cdot \mathbf{c} & 0 & -\mathbf{P}_{\sigma}^{\text{ref}} \cdot \mathbf{c} \\ \mathbf{c} & 0 & -\mathbf{c} \\ 0 & 0 & Id \end{pmatrix} \tag{22}$$

in the case of reference feedback and

$$\tilde{\mathbf{P}}_{\tilde{\mathbf{x}}}(\tilde{\mathbf{x}}^{\text{ref}}) \cdot \tilde{\mathbf{g}}_{\text{control},\tilde{\mathbf{x}}}(\tilde{\mathbf{x}}^{\text{ref}}) = \begin{pmatrix} \mathbf{P}_{\mathbf{x}}^{\text{ref}} + \mathbf{P}_{\sigma}^{\text{ref}} \cdot \mathbf{c} & 0 & -\mathbf{P}_{\sigma}^{\text{ref}} \cdot \mathbf{c} \\ \mathbf{c} & 0 & -\mathbf{c} \\ Id & 0 & 0 \end{pmatrix} \tag{23}$$

in the case of delay feedback. For example, the nontrivial eigenvalues of these matrices are given by the roots of the equation

$$|\mathbf{P}_{\mathbf{x}}^{\text{ref}} + \mathbf{P}_{\sigma}^{\text{ref}} \cdot \mathbf{c} - \lambda Id| = 0, \tag{24}$$

in the case of reference feedback and

$$|\lambda^2 Id - \lambda(\mathbf{P}_{\mathbf{x}}^{\text{ref}} + \mathbf{P}_{\sigma}^{\text{ref}} \cdot \mathbf{c}) + \mathbf{P}_{\sigma}^{\text{ref}} \cdot \mathbf{c}| = 0 \tag{25}$$

in the case of delay feedback.

Since $\mathbf{P}(\mathbf{x}, \sigma)$ lies on $\mathcal{P}_{\text{control}}$, it follows that the first row of $\mathbf{P}_{\mathbf{x}}^{\text{ref}}$ and $\mathbf{P}_{\sigma}^{\text{ref}}$ must equal zero. Consequently, the first row of $\mathbf{P}_{\sigma}^{\text{ref}} \cdot \mathbf{c}$ must also equal zero. It is now straightforward to show that there are only two nontrivial eigenvalues in the case of reference feedback and only three nontrivial eigenvalues in the case of delay feedback. In contrast, as the first component of $\mathbf{x} - \mathbf{x}^*$ automatically equals zero on $\mathcal{P}_{\text{control}}$, it follows that only the last two components of $\mathbf{c}$ remain to affect the local stability of the periodic trajectory. In the case of reference feedback, it is, in fact, possible to express the components of $\mathbf{c}$ in terms of a pair of desirable

eigenvalues (except for a restricted set of numerical values for the components of $\mathbf{P}_{\mathbf{x}}^{\mathrm{ref}}$ and $\mathbf{P}_{\sigma}^{\mathrm{ref}}$) although we refrain from showing the explicit formulas. As the number of eigenvalues in the case of delay feedback exceeds by one the number of control parameters, there are no such corresponding expressions in the case of delay feedback.

To improve on the local control strategy discussed here and, in particular, to be able to fully control the eigenvalues associated with delay feedback due to its desirable independence of $\mathbf{x}^{\mathrm{ref}}$, the jump function associated with delay feedback is modified to

$$\tilde{\mathbf{g}}_{\mathrm{control}}(\tilde{\mathbf{x}}) = (\mathbf{x}\ \sigma + c_{\sigma}(\sigma - \sigma^{\mathrm{ref}}) + \mathbf{c}\cdot(\mathbf{x} - \mathbf{x}^{*})\ \mathbf{x})^{T}, \qquad (26)$$

where $c_{\sigma} \neq 0$ is an additional control value (the previous formulation corresponds to the special case $c_{\sigma} = -1$). It now follows that the local flow near the periodic trajectory is to lowest order captured by the matrix

$$\tilde{\mathbf{P}}_{\tilde{\mathbf{x}}}(\tilde{\mathbf{x}}^{\mathrm{ref}}) \cdot \tilde{\mathbf{g}}_{\mathrm{control},\tilde{\mathbf{x}}}(\tilde{\mathbf{x}}^{\mathrm{ref}}) = \begin{pmatrix} \mathbf{P}_{\mathbf{x}}^{\mathrm{ref}} + \mathbf{P}_{\sigma}^{\mathrm{ref}} \cdot \mathbf{c} & (1 + c_{\sigma})\mathbf{p}_{\sigma}^{\mathrm{ref}} & -\mathbf{P}_{\sigma}^{\mathrm{ref}} \cdot \mathbf{c} \\ \mathbf{c} & 1 + c_{\sigma} & -\mathbf{c} \\ Id & 0 & 0 \end{pmatrix}. \qquad (27)$$

It is straightforward to show that there are again only three nontrivial (nonzero) eigenvalues of this matrix. It is now possible to express the last two components of $\mathbf{c}$ and the control parameter c_{σ} in terms of a triplet of desirable eigenvalues (except for a restricted set of numerical values for the components of $\mathbf{P}_{\mathbf{x}}^{\mathrm{ref}}$ and $\mathbf{P}_{\sigma}^{\mathrm{ref}}$) although we again refrain from showing the explicit formulas. For example, it is now typically possible to achieve a superstable periodic trajectory by selecting values for the control parameters that yield all zero eigenvalues. (Some further properties of the local control strategies are considered in the Appendix.)

3.2 Global Control. The linear nature of the local control strategies discussed in the previous section limits their applicability for global control purposes. For example, while it may be possible to switch between different periodic motions by manipulating $\mathbf{c}$ and $\mathbf{x}^{*}$ in the case of reference feedback and c_{σ} and $\mathbf{c}$ in the case of delay feedback (cf. [2]), the transitions are typically accompanied by significant transients.

To address the need for a global control strategy, the idea of approximating the global Poincaré map $\tilde{\mathbf{P}}(\tilde{\mathbf{x}})$ by a cell mapping [8] defined on (a subset of) $\mathcal{P}_{\mathrm{control}}$ is proposed. Specifically, attention is restricted to points on $\mathcal{P}_{\mathrm{control}}$ that lie on trajectories that impact the front and back stops only once before again returning to $\mathcal{P}_{\mathrm{control}}$. A rectangular grid is introduced on the set of allowable initial conditions and the grid cells are numbered appropriately. Each cell is then associated with the number of the cell within which the trajectory based at the center of the original cell intersects $\mathcal{P}_{\mathrm{control}}$ after one iteration. The corresponding mapping is clearly a discrete approximation to the global Poincaré map $\tilde{\mathbf{P}}$. Here, approximation errors arise from the fact that the images of all points in a cell under $\tilde{\mathbf{P}}$ are approximated by the image of the center point. Such errors are thus related to the grid resolution and the nonlinearity of the dynamical system.

The approximate Poincaré map obtained through the cell map technique can now be combined with either or both of the local control strategies to yield a global control scheme. Here, the cell map data are mined to find an appropriate value of σ that will result in a desirable value of $\mathbf{x}$ at the next intersection with $\mathcal{P}_{\mathrm{control}}$ that is suitable for subsequent application of the local strategies. The possibility of using the cell map information to control the value of $\mathbf{x}$ several iterates downstream is typically compromised by the loss of accuracy associated with the grid resolution.

4 Numerical Results

The performance of the control scheme proposed above is illustrated by considering the possibility of generating a predetermined sequence of high- and low-velocity impacts between the hammer and the front stop. This corresponds to a working scenario under which the position of the back stop is used to select between impacts that will generate a dot on the paper and impacts that will not.

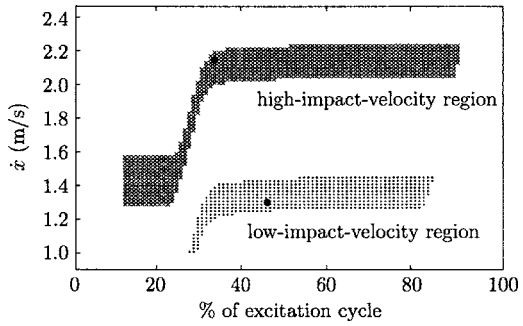

Fig. 4 The backward-in-time images of trajectories based at initial conditions at the front stop with strong (high impact velocity) and weak (low impact velocity) impacts under the free-flight flow. Here, the dots refer to the location of periodic system responses.

Let $\sigma^{\mathrm{ref}} = 0$ mm, $T_{\mathrm{lag}} = 0.00165$ s, and $d = 2.5$ mm. Denote impacts with impact velocities in the range [2.0, 2.2] as "strong" and in the range [1.1, 1.5] as "weak." The backward-in-time images of these regions under the free-flight flow are shown in Fig. 4. Here we again omit trajectories that impact more than once in forward time prior to returning to $\mathcal{P}_{\mathrm{control}}$.

For the chosen parameter values there exist a high-impact-velocity stable periodic trajectory at

$$\mathbf{x}_{1}^{\mathrm{ref}} \approx (0.0025\ 2.14\ 0.00252)^{T}, \qquad (28)$$

such that

$$\mathbf{P}_{\mathbf{x}}^{\mathrm{ref}_1} \approx \begin{pmatrix} 0 & 0 & 0 \\ 68.4 & 0.1168 & -154.4 \\ -0.00632 & -0.0001079 & 0.1427 \end{pmatrix}, \qquad (29)$$

$$\mathbf{P}_{\sigma}^{\mathrm{ref}_1} \approx \begin{pmatrix} 0 \\ 462 \\ -0.800 \end{pmatrix}, \qquad (30)$$

and a low-impact velocity unstable periodic trajectory at

$$\mathbf{x}_{2}^{\mathrm{ref}} \approx (0.0025\ 1.32\ 0.00350)^{T}, \qquad (31)$$

such that

$$\mathbf{P}_{\mathbf{x}}^{\mathrm{ref}_2} \approx \begin{pmatrix} 0 & 0 & 0 \\ 623 & 1.231 & -748 \\ 1.041 & -0.00206 & 1.250 \end{pmatrix}, \qquad (32)$$

$$\mathbf{P}_{\sigma}^{\mathrm{ref}_2} \approx \begin{pmatrix} 0 \\ 1147 \\ -2.53 \end{pmatrix} \qquad (33)$$

(cf. Fig. 4).

For each of these periodic trajectories, the linear approximations afforded by Eqs. (22) and/or (27) may be used to arrive at values for the gain parameters $\mathbf{c}$ and c_{σ}. As indicated previously, closed-form expressions may be obtained for the gain parameters in terms of a set of desirable eigenvalues. For example, all zero eigenvalues in the case of delay feedback correspond to

$$c_2 = 0.0000598, \quad c_3 \approx -0.0791, \quad c_{\sigma} \approx -1.350 \qquad (34)$$

for the high-impact trajectory and

$$c_2 \approx -0.000926, \quad c_3 \approx 0.397, \quad c_\sigma \approx 0.0844, \tag{35}$$

for the low-impact trajectory. Similarly, in the case of reference feedback, closed-form expressions may be obtained for the gain parameters that minimize the ratio between the distance from $\mathbf{x}^{\text{ref}}$ at subsequent intersections with $\mathcal{P}_{\text{control}}$. For example, defining the distance by $\sqrt{\Delta\dot{x}^2+500\Delta\theta^2}$, where $\theta=t$ modulo the period T of the excitation, yields

$$c_2 \approx -0.000202, \quad c_3 \approx 0.268 \tag{36}$$

for the high-impact trajectory and

$$c_2 \approx -0.000931, \quad c_3 \approx 0.566 \tag{37}$$

for the low-impact trajectory.

Finally, construct a cell mapping on a $40\times80\times40$ rectangular grid on the volume $1.0\leqslant\dot{x}\leqslant3.0$, $0\leqslant\theta/T\leqslant1$, and $-0.002\leqslant\sigma\leqslant0.002$.

The existence of the periodic trajectories in the high- and low-impact-velocity regions in Fig. 4 suggests using the cell map data to reach a local neighborhood of the desirable periodic trajectory and the local control to remain within this neighborhood. Here, the nonlocal strategy is designed to select the value of σ that (i) lies inside the corresponding region in Fig. 4 and (ii) minimizes the distance (as defined above) to the appropriate periodic trajectory. Moreover, once inside the local neighborhood of the desirable periodic trajectory, reference feedback using the above gain parameter values is applied at most three consecutive iterations, after which delay feedback is applied using the above gain parameter values. It is assumed that $|\sigma|$ may not exceed 2 mm and that the extreme value is used whenever the feedback suggests a value of $|\sigma|$ larger than 2 mm.

Consider, as an example, the impact pattern

$$0-1-1-0-0-0-0-0-0-1-1-1$$

where 1 represents a strong impact and 0 a weak impact. Figures 5 and 6 show the time evolution of $\dot{x}$, 0, and σ for the desired impact pattern using reference feedback along and using the combined control scheme, respectively. Here, we note that while reference feedback is able to achieve a switch between the low- and high-impact-velocity regions, this is accompanied by significant transients, especially when attempting to reach the high-impact-velocity region. In contrast, the combined control scheme is able to eliminate these transients in favor of a rapid convergence toward the desired periodic trajectory.

5 Discussion

The control strategy implemented here offers an alternative to the operating mode of existing impact-hammer based printing devices. Where current devices use the transient dynamics of the impact hammer to achieve a desirable impact velocity, assuming that the hammer essentially comes to rest in between pulses, the proposed strategy relies on the existence of desirable recurrent motions for the uncontrolled system. Indeed, in current designs, part of the energy injected into the hammer from the coil current is used to overcome static friction. As the proposed strategy relies on keeping the hammer in constant motion, this is avoided. On the other hand, the proposed strategy may result in higher heat generation than the current control strategy as it keeps the current pulses coming even when the hammer is in the weak-impact mode.

The success of the proposed scheme suggests the possibility of redesigning the back stop to reduce the amount of energy lost in collisions of the impact hammer with the back stop. Coupled with a reduction in the amplitude of the current pulse, this might allow for a switching between strong and weak (or no) impacts with an overall reduction in energy consumption and subsequent heat generation. This is clearly an area for more careful study and should be integrated with a careful discussion of the practical means by which both the sensing (corresponding to $\mathcal{P}_{\text{control}}$) and the control (for example, using stacked, amplified piezoactive actuators for stroke lengths up to fractions of 1 mm) can be implemented in an actual impact hammer.

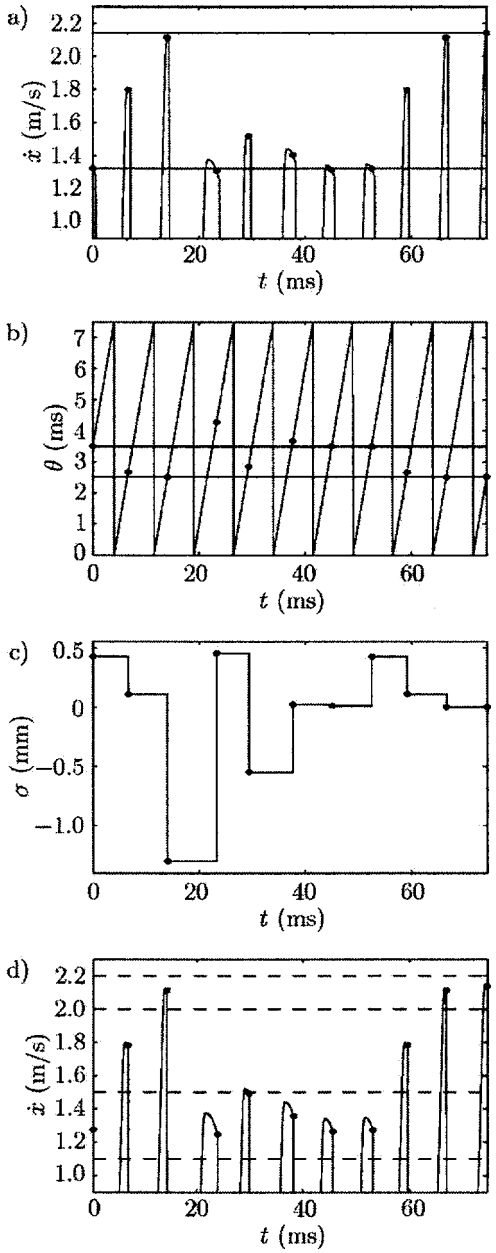

Fig. 5 Dynamic response of the impact hammer under reference feedback only. Here, the desired impact pattern 0-1-1-0-0-0-0-0-1-1-1 governs the switch between the appropriate values of $\mathbf{x}^{\text{ref}}$ and the associated gain parameter values. Specifically, panels (*a*) and (*d*) depict the time evolution of the hammer velocity including discrete points representing the velocity at the Poincaré section (Panel (*a*)) and the velocity at the impact with the front stop (Panel (*d*)). Panels (*b*) and (*c*) show the time evolution of θ and σ, respectively, including discrete points representing their values upon leaving the Poincaré section, i.e., after the imposition of $\tilde{\mathbf{g}}_{\text{control}}$.

Acknowledgment

The financial support of the Swedish Research Council and the National Science Foundation, Division of Civil and Mechanical Systems, Grant No. 0237370, is gratefully acknowledged.

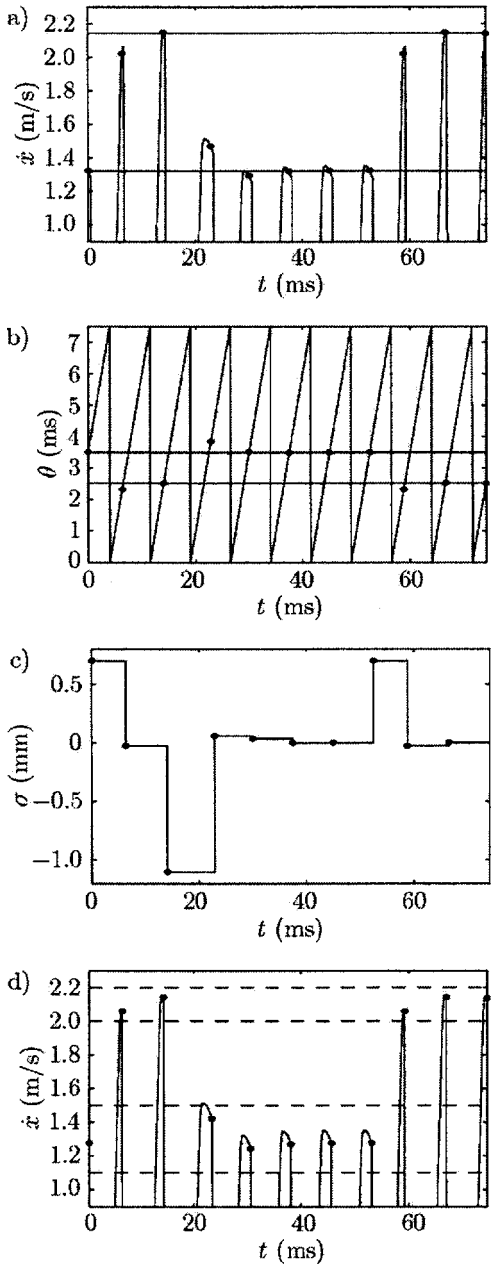

Fig. 6 Dynamic response of the impact hammer under the combined control scheme. Here, the desired impact pattern 0-1-1-0-0-0-0-0-1-1-1 governs the switch between the appropriate values of $\mathbf{x}^{\text{ref}}$ and the associated gain parameter values. Specifically, panels (*a*) and (*d*) depict the time evolution of the hammer velocity including discrete points representing the velocity at the Poincaré section (panel (*a*)) and the velocity at the impact with the front stop (panel (*d*)). Panels (*b*) and (*c*) show the time evolution of θ and σ, respectively, including discrete points representing their values upon leaving the Poincaré section, i.e., after the imposition of $\tilde{\mathbf{g}}_{\text{control}}$.

Nomenclature

$x, \dot{x}, \ddot{x}$ = displacement, velocity and acceleration of the core
t = time
m_{core} = mass of core
m_{fs} = mass of front stop
m_{bs} = mass of back stop
k = stiffness of helical spring
k_{fs} = stiffness of front stop
$k_{\text{bs},1}, k_{\text{bs},2}$ = stiffness of back stop
c_{fs} = damping of front stop
c_{bs} = damping of back stop
s = position of front stop
σ = position of back stop
d_{spring} = initial deformation of the spring
d_{fs} = initial deformation of the front stop
L, L_0, L_1 = coil inductance
$I(t)$ = current
T_{lag} = lag time between current pulses

Appendix

The linear control strategies discussed in this paper are characterized in the context of the local stability of an existing (and persistent) periodic trajectory of the uncontrolled system. As suggested above, it is possible to select numerical values for the control parameters that will result in arbitrary eigenvalues for the linearization about the periodic trajectory. Indeed, as long as the resultant nontrivial eigenvalues are kept away from 1, the implicit function theorem guarantees that there are no additional periodic trajectories with a single intersection with the Poincaré section $\mathcal{P}_{\text{control}}$ in some neighborhood of $\tilde{\mathbf{x}}^{\text{ref}}$. The implicit function theorem does not, however, make any claims regarding the global behavior of the controlled system.

Consider, for example, the dynamical system obtained by applying reference feedback with a particular value of σ^{ref} to the original system for arbitrary values of $\mathbf{x}$ on $\mathcal{P}_{\text{control}}$. Then, for a periodic trajectory of this system with a single intersection $\tilde{\mathbf{x}} = (\mathbf{x}\ \sigma\ \mathbf{x}^*)^T$ with $\mathcal{P}_{\text{control}}$

$$\tilde{\mathbf{x}} = \begin{pmatrix} \mathbf{P}(\mathbf{x},\sigma) \\ \sigma^{\text{ref}} + \mathbf{c}\cdot(\mathbf{P}(\mathbf{x},\sigma) - \mathbf{x}^*) \\ \mathbf{x}^* \end{pmatrix}. \tag{A1}$$

It follows that $\mathbf{x}$ must lie on a periodic trajectory of the uncontrolled system with $\sigma = \sigma^{\text{ref}} + \mathbf{c}\cdot(\mathbf{x} - \mathbf{x}^*)$ for some $\mathbf{x}^*$. In contrast, in the case of delay feedback, for a periodic trajectory with a single intersection $\tilde{\mathbf{x}} = (\mathbf{x}\ \sigma\ \mathbf{x}^*)^T$ with $\mathcal{P}_{\text{control}}$

$$\tilde{\mathbf{x}} = \begin{pmatrix} \mathbf{P}(\mathbf{x},\sigma) \\ \sigma + c_\sigma(\sigma - \sigma^{\text{ref}}) + \mathbf{c}\cdot(\mathbf{P}(\mathbf{x},\sigma) - \mathbf{x}^*) \\ \mathbf{P}(\mathbf{x},\sigma) \end{pmatrix}. \tag{A2}$$

It follows that $\mathbf{x}$ must lie on a periodic trajectory of the uncontrolled system with $\sigma = \sigma^{\text{ref}}$. Thus, while new periodic trajectories with a single intersection with $\mathcal{P}_{\text{control}}$ may occur in the controlled system with reference feedback, this cannot happen with delay feedback. Similar conclusions hold for periodic trajectories with multiple intersections with $\mathcal{P}_{\text{control}}$.

References

[1] Jerrelind, J., and Stensson, A., 1999, "Braille Printer Dynamics," *Proc. ASME DETC99*, Las Vegas, Paper No. DETC99/VIB-8032.
[2] Jerrelind, J., and Dankowicz, D., 2003, "Low-Cost Control of Impact Hammer Performance," *Proc. of ASME DETC03*, Chicago, Paper No. DETC2003/VIB-48486.
[3] Hendriks, F., 1983, "Bounce and Chaotic Motion in Impact Print Hammers," IBM J. Res. Dev., **27**(3), pp. 273–280.
[4] Tung, P. C., and Shaw, S. W., 1988, "The Dynamics of an Impact Print Hammer," ASME J. Vib., Acoust., Stress, Reliab. Des., **110**, pp. 193–200.
[5] Springer, H., and Ullrich, M., 1990, "Dynamics of Dot-Matrix Printers," in *Nonlinear Dynamics in Engineering systems*, W. Schiehlen, ed., Springer, Berlin, pp. 297–304.
[6] Tung, P. C., and Shaw, S. W., 1988, "A Method for the Improvement of Impact Printer Performance," ASME J. Vib., Acoust., Stress, Reliab. Des., **110**, pp. 528–532.
[7] Dankowicz, H., and Piiroinen, P. T., 2002, "Exploiting Discontinuities for Stabilization of Recurrent Motions," Dyn. Syst., **17**(4), pp. 317–342.
[8] Hsu, C., 1980, "Theory of Cell-to-Cell Mapping Dynamical Systems," J. Appl. Mech., **47**, pp. 931–939.